

Robustness of Binary Black Hole Mergers in the Presence of Spurious Radiation

Tanja Bode,¹ Deirdre Shoemaker,^{1,*} Frank Herrmann,¹ and Ian Hinder¹

¹*Center for Gravitational Wave Physics,
The Pennsylvania State University, University Park, PA 16802, USA*

(Dated: September 19, 2021)

We present an investigation into how sensitive the last orbits and merger of binary black hole systems are to the presence of spurious radiation in the initial data. Our numerical experiments consist of a binary black hole system starting the last couple of orbits before merger with additional spurious radiation centered at the origin and fixed initial angular momentum. As the energy in the added spurious radiation increases, the binary is invariably hardened for the cases we tested, i.e. the merger of the two black holes is hastened. The change in merger time becomes significant when the additional energy provided by the spurious radiation increases the Arnowitt-Deser-Misner (ADM) mass of the spacetime by about 1%. While the final masses of the black holes increase due to partial absorption of the radiation, the final spins remain constant to within our numerical accuracy. We conjecture that the spurious radiation is primarily increasing the eccentricity of the orbit and secondarily increasing the mass of the black holes while propagating out to infinity.

PACS numbers: 04.25.dg,04.30.Db,04.70.Bw

I. INTRODUCTION

The coalescence of two black holes, long thought of as the “holy grail” of numerical relativity (NR), is well on its way to being a solved problem. Many groups in NR have now demonstrated the ability to follow two black holes through several orbits [1] and their final orbits and merger to a single black hole [2, 3, 4, 5, 6, 7, 8]. From the first published waveform of equal-mass, non-spinning binary black hole (BBH) coalescence, the simplicity of the waveform’s dependence on time has been noted. Comparisons amongst the groups in NR have demonstrated a remarkable agreement to the solution of the BBH problem. A common aspect in all numerical relativity BBH evolutions is the presence of spurious radiation in the initial data. In this paper, we present a study on how the standard equal-mass, quasi-circular BBH system responds to the presence of spurious radiation that has been added in a controlled manner and map that response as a function of the radiation’s initial conditions. Our intent is to determine how much junk radiation the system can handle and how the waveforms and the physical properties of the final black hole deviate from the standard BBH result.

Several papers have compared BBH waveforms. One of the first papers to internally compare waveforms also demonstrated the first evidence of “universality” [9] in an equal-mass, non-spinning initial configuration. The paper demonstrated that differences in initial data characterized by a change in the initial orbital separation manifested as a time shift in the amplitude and phase of the gravitational waveforms. Once time-shifted, the waveforms were within 1% agreement over the merger and ringdown in $|r_0\Psi_4|$. We investigate the effect that the additional spurious radiation we add to the binary will have on this universality.

The first comparison of NR waveforms between several groups [10] includes the most popular methods used in the community to evolve BBHs covering excision with a hyperbolic formulation [2] and moving punctures with the Baumgarte-Shapiro-Shibata-Nakamura (BSSN) formulation of the Einstein equation [3, 4]. The waveforms were in remarkable agreement once time-shifted, the largest differences, occurring at the beginning of the wave, being due to the spurious radiation in the initial data. A second, independent comparison of waveforms from different methods was conducted by Spermhake [11] in which he compared a Kerr-Schild/excision evolution to a puncture evolution within the same code. An interesting issue to investigate is to what extent the spurious radiation in the initial data could cause differences in the merging time and thus affect waveform com-

*Also at Department of Physics and Institute for Gravitation and the Cosmos, The Pennsylvania State University, University Park, PA 16802, USA

parisons based on time-shifts to align the amplitude of the waveform.

Most groups remove the initial burst from the waveform during post-processing of the data [12, 13]. From the evolutions published, it appears that the spurious radiation that is present in the initial data is flushed out of the system within a crossing time, leaving the binary dynamics mostly untouched. There is still some concern about the impact that choices made in setting up the initial data for the evolutions, choices like conformal flatness, have on the waveforms. Studies have looked at different ways of choosing the freely specifiable part of initial data [14] which reduce the amplitude of the spurious radiation, but these have not been extensively implemented in evolutions.

In this paper, we test the robustness of the binary to effects of spurious radiation. We create a BBH system containing additional radiation with tunable initial energy initialized at the binary's center of mass. We then evolve a series of equal-mass, non-spinning, quasi-circular BBH plus radiation spacetimes using the PSU numerical code that implements the *Moving Puncture Recipe* (MPR) [3, 4], see [15] for details about the PSU code. The initial data used to construct the BBH plus radiation spacetime is presented in Section III, the results in Section IV and the conclusions in Section V. Our main result is that the presence of spurious radiation causes a hastening of the merger, thus plausibly accounting for the differences in merger times seen in the NR waveform comparisons. Before describing our numerical experiment, we present a back-of-the-envelope calculation to build our intuition about this problem.

II. A NEWTONIAN PERSPECTIVE

For illustrative purposes, we investigate the effect a central pulse of energy might have on a binary by studying a two-body orbit in Newtonian gravity with a stationary mass placed at the orbit's center of motion while the bodies are at their apocenter. The addition of the third mass at the center of the Newtonian binary affects the orbit by deepening the potential in which the binary sits. We solve the problem using the standard central force solution to the two-body problem with the new potential. We assume $\dot{r} = 0$ initially since this is set in the parameters to the initial data solver. Letting m be the masses of the black holes and

m_w be the equivalent mass of the third body, we write the ratio of the final eccentricity, e' , to the original eccentricity as

$$\left(\frac{e'}{e}\right)^2 = \frac{1}{(1+2f)^2} \left[1 + \frac{(4-2j^2/\mu d)f + 4f^2}{e^2} \right] \quad (1)$$

where $f = m_w/m$ is the fractional mass, $j = l/\mu$ is the angular momentum per unit reduced mass, and d is the initial separation of the binary.

This simple calculation indicates that the eccentricity increases for sufficiently small eccentricities. For the binary parameters studied in this paper, the eccentricity invariably increases for $e \leq 0.88$. Although the black holes in our BBH evolutions are not far enough apart to allow a valid determination of eccentricity, the trajectories are quasi-circular enough for the eccentricity to be low. This illustrates that we can expect the addition of radiation into the studied system to cause the binary's orbit to become more elliptic.

III. INJECTING RADIATION INTO A BBH EVOLUTION

We inject radiation into the standard, equal-mass, non-spinning, quasi-circular BBH evolution during the setup of the initial data. The initial data for the evolution is constructed via the puncture method [16] using the single-domain spectral method code developed by Ansorg et al. [17] that uses a conformally flat prescription to solve the constraints. We have two building blocks for the data: 1) the quasi-circular BBH and 2) the tunable radiation. The BBH data is set-up using the input conditions for the Baker et al. [9] R1 run of two equal-mass irrotational black holes in quasi-circular orbits such that the metric is conformally flat. The details of the R1 initial data are given in the first row of Table I and a convergence study was done in [15].

A. The Teukolsky-Nakamura Wave

The tunable radiation is given by an even parity, quadrupolar gravitational wave: the linearized solution to a perturbation on Minkowski spacetime expanded over the modes of the Mathews tensor spherical harmonics [18]. This radiation was first derived by Teukolsky [19] and is typically known as a Teukolsky wave. This tensor is

simply the general traceless-transverse solution to the linearized Einstein equation. Nakamura [20] later wrote out the solution for general ℓ and m . Instead of using that tensor as a metric perturbation, he used it as an extrinsic curvature perturbation. We implement the Nakamura version

of the Teukolsky wave, herein called Teukolsky-Nakamura waves (TNWs), in order to satisfy the condition of a conformally flat metric imposed by the puncture method.

The Teukolsky-Nakamura (TN) extrinsic curvature tensor is given by

$$\tilde{A}_{ij}^{\text{TN}} = \sum_{l,m} \begin{pmatrix} a_{lm} Y_{lm} & b_{lm} Y_{lm,\theta} & b_{lm} Y_{lm,\varphi} \\ & g_{lm} Y_{lm} + f_{lm} W_{lm} & f_{lm} X_{lm} \\ & & (g_{lm} Y_{lm} - f_{lm} W_{lm}) \sin^2 \theta \end{pmatrix} \quad (2)$$

where the coefficients a_{lm} , b_{lm} , f_{lm} , and g_{lm} are functions only of r and t as follows

$$a_{lm} = r^{l-2} \left(\frac{1}{r} \frac{\partial}{\partial r} \right)^l \frac{F(t-r) + F(t+r)}{r}, \quad (3a)$$

$$b_{lm} = \frac{1}{l(l+1)r} \frac{\partial}{\partial r} (r^3 a_{lm}), \quad (3b)$$

$$g_{lm} = -\frac{r^2}{2} a_{lm}, \quad (3c)$$

$$f_{lm} = \frac{1}{(l-2)(l+1)} \left[g_{lm} + \frac{\partial}{\partial r} \left(\frac{r}{l(l+1)} \frac{\partial}{\partial r} (r^3 a_{lm}) \right) \right] \quad (3d)$$

and the angular functions X_{lm} and W_{lm} are

$$X_{lm} = 2 \frac{\partial}{\partial \varphi} \left(\frac{\partial}{\partial \theta} - \cot \theta \right) Y_{lm}, \quad (4a)$$

$$W_{lm} = \left(\frac{\partial^2}{\partial \theta^2} - \cot \theta \frac{\partial}{\partial \theta} - \frac{1}{\sin^2 \theta} \frac{\partial^2}{\partial \varphi^2} \right) Y_{lm}. \quad (4b)$$

Note that the TN solution lets us choose the radial dependence in the form of ingoing and outgoing functions which we have chosen to be the same symmetric functional form, $F(u)$. $F(u)$ is given by an Eppley packet [21]

$$F(u) = A u e^{-u^2/\sigma^2}, \quad (5)$$

where $u = t \pm r$. The Eppley packet is localized and smooth with the factor of u present so the wave is more regular at the origin. Later in the paper we investigate a cosine modulation of this function. We can choose the location, mode content, strength, and radial dependence of the injected radiation. Since the extrinsic curvature is real and the spherical harmonics are complex, we take only the real part of the X_{lm} tensor resulting in a superposition of m and $-m$ modes in the TNW.

B. BBH+TNW

Our initial data, the spatial metric and extrinsic curvature, are given by

$$g_{ij} = \psi^4 \eta_{ij}, \quad (6a)$$

$$K_{ij} = \psi^{-2} (\tilde{A}_{ij}^{BY} + \tilde{A}_{ij}^{\text{TN}}), \quad (6b)$$

where η_{ij} is the flat spatial metric and ψ is the solution to the Hamiltonian constraint under York's conformal approach [22]. The extrinsic curvature \tilde{A}_{ij}^{BY} is the Bowen and York solution [23] to the momentum constraint and $\tilde{A}_{ij}^{\text{TN}}$ is the TN tensor. Notice that because the momentum constraint is linear in the extrinsic curvature, the superposition of the extrinsic curvature is also a solution of the momentum constraint. As a test we evolved the above initial data with a vanishing Bowen-York

tensor, i.e. Minkowski background. For the $\ell = 2$, $m = \pm 2$ case, we found that the Arnowitt-Deser-Misner (ADM) angular momentum calculated on the initial spacetime is zero to within machine error. The angular momentum of the BBH+TNW is therefore independent of the TNW to our numerical accuracy.

C. Configurations

The simplest geometry to add additional spurious radiation to our BBH initial data is to center a wave pulse at the origin. We typically choose an $\ell = 2$, $m = 2$ mode, the dominant mode for gravitational radiation from a BBH system, and vary the amplitude, A , and width, σ , of the Eppley packet. The values of σ/M are chosen from the set $\{0, 3, 4, 5, 6\}$ and those of the amplitude A/M^3 from the set $\{0, 0.1, 0.5, 1.0, 1.5\}$ where the dry R1 BBH spacetime is recovered when $A/M^3 = 0$. Fig. 1 shows the shape of the wave in one of the components of the traceless-transverse extrinsic curvature, $A_{ij} = \psi^{-2} \tilde{A}_{ij}$, along the coordinate axis intersecting the two black holes, modulated by the inverse square of the conformal factor, for $A = 1M^3$ and $\sigma = 3M, 4M, 5M, 6M$.

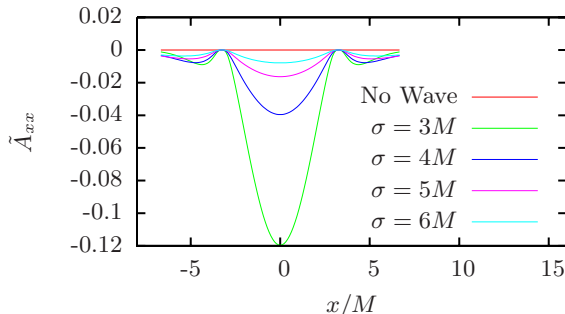


FIG. 1: Comparison of \tilde{A}_{xx} initially between various Eppley packet widths, σ , for a wave amplitude of $1M^3$. This is from the binary black hole initial data where \tilde{A}_{xx} vanishes at the punctures.

When adding the TNW to the spacetime we wanted to keep the initial black holes unaltered. We chose to keep the apparent horizon (AH) masses constant independent of the additional wave content. In practice the AH masses varied by as much as 0.04% from the dry R1 run due to insufficient parameter accuracy. The momenta remain constant as parameters to the initial data

solver, and the ADM angular momentum differs by at most 0.001% from the dry R1 run. The second column of Table I lists the ADM energy of the spacetime for each wave choice. We note that the waves increase the ADM energy from a negligible $10^{-4}\%$ to a significant 8.9%, which scales empirically as $E_{\text{ADM}} \simeq A^2/\sigma^5$. The proper separation between the black holes changes from the dry case of $L = 9.94$ to a maximum of $L = 10.23$. In the most extreme case, the wave having $A = 1.5M^3$ and $\sigma = 3M$, we have added almost 9% additional energy into the BBH system and effectively moved the black holes apart by $0.29M$. The impact of these differences in initial data on the binary evolution are discussed further in the next section.

Pumping energy into the system while holding the coordinate separation and angular momentum constant necessarily means that we are changing the binding energy of the system. To study this change we map the effective potentials for each BBH+TNW case. We do this by repeatedly solving the initial data with incremented separations while holding the individual AH masses and total ADM angular momentum fixed. We calculated the quantity $E_b = E_{\text{ADM}} - m_{\text{AH},1} - m_{\text{AH},2}$ for each spacetime. The wave itself adds to the ADM energy and must be subtracted in this calculation; but, as we’re only interested in the relative shapes, we can look at the relative binding energy, $E_b - E_{b,\text{min}}$. For the waves with a σ of $4M$ the binding energy per unit reduced mass is plotted in Fig. 2 with a vertical line indicating the initial coordinate separation of the black holes. We can immediately see that the dry “quasi-circular” R1 case has some non-zero eccentricity as the imposed separation does not lie at the minimum of the curve. We also observe a shift of the minimum inwards as the wave strength increases. Since the coordinate separation in the parameter search is held fixed for the evolved initial data, the location of the system along the binding energy curve with respect to its minimum is sufficient to see that the eccentricity of the orbit is likely increasing. Unfortunately, the separation is too small to get a reliable measure of the eccentricity.

IV. EVOLUTIONS OF THE BBH+TNW

Our simulations of the BBH+TNW initial data are summarized in Table I, where the first row corresponds to the BBH system without added radiation, the dry R1 run. This will be our control

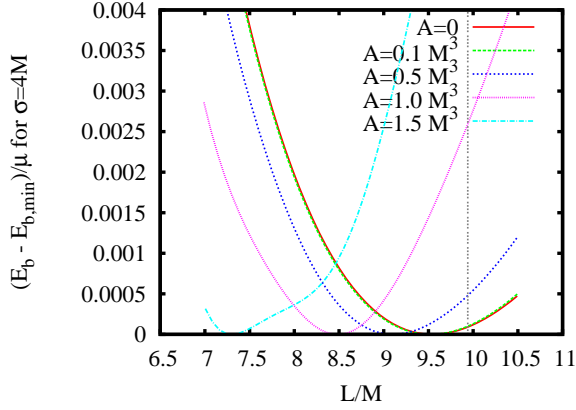


FIG. 2: We plot the effect of the wave on the binding energy per unit reduced mass in the initial data. The potentials were calculated by solving the initial data using Ansorg’s code for various separations while keeping the individual AH masses and total ADM angular momentum fixed.

case. We systematically evolved each BBH+TNW spacetime, varying A and σ of the TNW. We divide the results from evolving these simulations into four subsections: the main result concerning the merger time in § IV A, the dynamical and radiated quantities from our runs are in § IV B, the final spacetime quantities in § IV C, and a comparison of the gravitational waves by time-shifting in § IV D.

A. Merger Time

The main result of adding gravitational radiation to our BBH evolution is to hasten the merger of the black holes. With increasing E_{ADM} , the binary invariably merges *faster*. The sixth column in Table I lists the differences in merger times between the dry R1 and the BBH+TNW runs given by $\Delta T = (T_0 - T_{0,\text{dry}})/M$. The time, T_0 , is given in units of the total, initial AH masses of the black holes and evaluated at the peak amplitude of each waveform extracted at a radius of $75M$. The use of the waveform peak variation as a measure of the change in merger time agrees within a few percent in ΔT to the variation in the time it takes for the punctures to be separated by one grid spacing.

Figs. 3 and 4 show the change in merger times from the perspective of constant wave amplitude and constant pulse width. We can see that there is

		Run Quantities					
A/M^3	σ/M	E_{ADM}	$\frac{E_{\text{rad}}}{E_{\text{ADM}}}$	$\frac{J_{\text{rad}}}{J_{\text{ADM}}}$	$\Delta T/M$	M_f	j_f
0.0	0	0.9957	0.0359	0.273	0.0	0.9599	0.682
0.1	3	0.996	0.0363	0.273	-0.6	0.9600	0.683
0.5	3	1.007	0.0451	0.271	-16.4	0.9609	0.682
1.0	3	1.037	0.0708	0.263	-56.1	0.9635	0.686
1.5	3	1.084	0.1058	0.244	-88.4	0.9696	0.693
0.1	4	0.996	0.0360	0.274	+1.5	0.9596	0.682
0.5	4	0.999	0.0385	0.272	-4.7	0.9604	0.682
1.0	4	1.007	0.0463	0.272	-14.3	0.9603	0.683
1.5	4	1.021	0.0589	0.270	-31.8	0.9607	0.683
0.1	5	0.996	0.0360	0.273	+0.2	0.9599	0.682
0.5	5	0.997	0.0369	0.273	-0.1	0.9599	0.682
1.0	5	1.000	0.0399	0.272	-4.6	0.9603	0.683
1.5	5	1.005	0.0448	0.272	-7.8	0.9599	0.686
0.1	6	0.996	0.0359	0.273	+0.2	0.9599	0.682
0.5	6	0.996	0.0364	0.273	+0.7	0.9599	0.682
1.0	6	0.998	0.0377	0.273	-0.3	0.9601	0.682
1.5	6	1.000	0.0399	0.272	-2.2	0.9602	0.682

TABLE I: The first two columns are the parameters of the TNWs followed by the ADM energy of the initial spacetimes. Column 4 and 5 give the fraction of the ADM energy and angular momentum radiated over the simulation. Column 6 is the change in merger time calculated by the shift in extracted waveform peak in units of the total AH mass in the initial spacetime. Column 7 lists the final mass and Column 8 the final spin, $j_f = a_f/M_f$ of the black hole.

a strong dependence on the width of the pulse as well as the amplitude. Some cases show a positive value for ΔT ; however, these are all equal to zero within the errors. For all the $A = 1M^3$ waves that have non-zero merger time we found an approximate power law relation between the width of the pulse and the change in merger time:

$$\Delta T(A = 1M^3) \propto \sigma^{-4.93}. \quad (7)$$

A more general look at the change in merger times is found in Fig. 5. Given our estimated error bars, significant changes in merger time occur when the TNW has increased the initial ADM energy of the spacetime by about 1% compared to that of the dry R1.

To isolate how much of ΔT is due to the additional spurious radiation introduced and how much is due to other factors, we perform a series of tests. We focus on the most significant sources of errors, namely the resolution of our grid, wave extraction radius, the change in proper distance in setting up the initial data, and the change in mass of the two black holes. We will look at each of these factors and assess their individual contri-

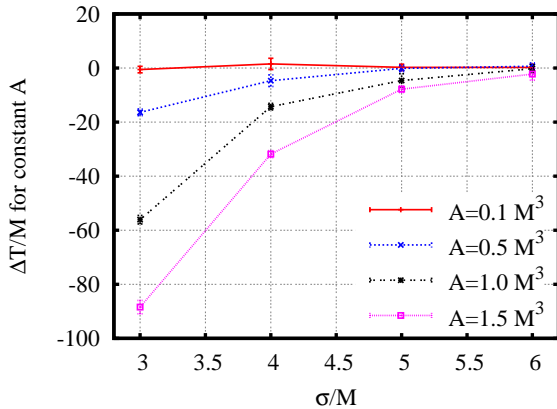


FIG. 3: Changes in merger times compared to the dry R1 run as a function of packet width with estimated error bars.

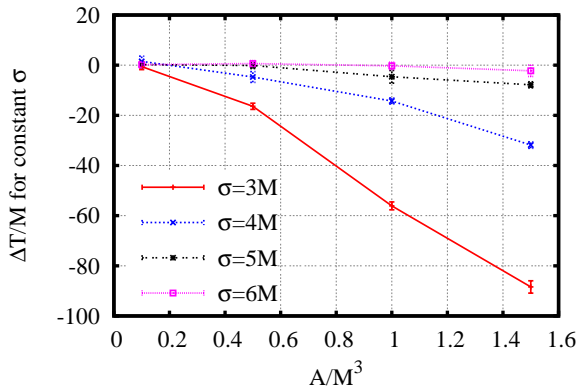


FIG. 4: Changes in merger times compared to the dry R1 run as a function of wave amplitude with estimated error bars.

bution to ΔT .

1. *Resolution:* The finest resolution for the simulations we present in Table I is $M/38.4$. We check the error due to the resolution by repeating several cases with finest resolutions of $M/44.8$ and $M/51.2$. We ran convergence tests on the strongest wave ($A = 1.5M^3$, $\sigma = 3M$) and the weakest wave ($A = 0.1M^3$, $\sigma = 6M$). A third, medium, wave with $A = 0.5M^3$ and $\sigma = 4M$ was run at just one more resolution, $M/44.8$. For all three cases, the merger time *decreased*. The merger time of the compact wave decreased little for a total of $0.1M$ over the three resolutions

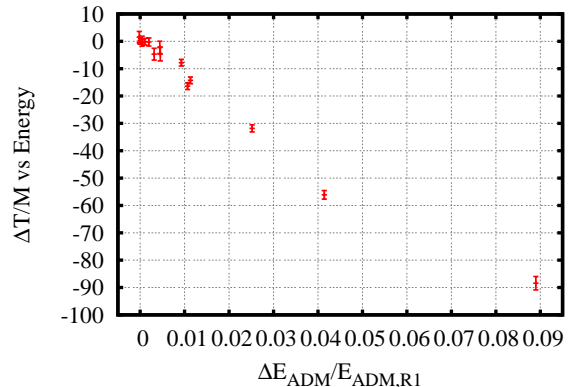


FIG. 5: Changes in merger times compared to the fractional change in initial ADM energy of the spacetime with estimated error bars.

while the diffuse wave decreased more drastically for a total of about $0.5M$. The medium case had a $0.2M$ difference between the two resolutions.

2. *Extraction Radius:* The next source of error is wave extraction radius. In NR, waveforms are usually calculated in terms of the Newman-Penrose scalar, $\Psi_4(t, x, y, z)$, which are extracted on a sphere at a finite radius some distance from the source, then expanded into angular modes via the spin-weighted spherical harmonics, ${}_{-2}Y_{\ell m}(\theta, \phi)$. With a proper choice of tetrad, this scalar is a measure of outgoing gravitational radiation. There has been recent work investigating the effects the choice of extraction radius can have on the correctness of the waveform [24, 25]. As the extraction radius increases, the errors caused by an incorrect tetrad and finite distance diminish. While it is still an open question whether or not there are observable effects from the methods groups currently use to extract the waveforms, the methodology of the extraction is not thought to contaminate the waveform. An indication the appropriate tetrad is being approached is that the waveform amplitude scales as $1/r$, which we tested. To get a rough estimate of the errors due to extracting at a finite radius, we compute ΔT using radiation extracted at $30M$ and extracted at $75M$. In Fig. 6 we plot the amplitude of the dominant waveform mode, $|\Psi_4^{2,2}|$, extracted at the two radii for both the dry R1 run and one where the merger time changed significantly. The merger time shift changed by no more than $0.4M$ between the two extraction radii.

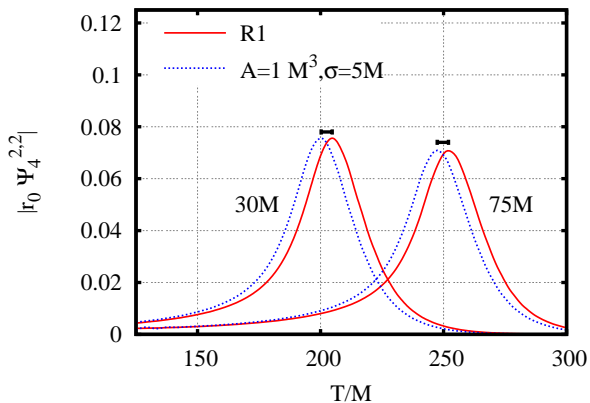


FIG. 6: Sample comparison of waveforms extracted at different radii. Plotted are the waveforms for the dry R1 run and $A = 1M^3$, $\sigma = 5M$ run extracted at $30M$ and $75M$.

3. *Black Hole Mass:* Aside from unphysical sources of error, the small differences in the initial data also change the merger time. Though we kept the initial AH masses nearly identical, there is still a variation of up to 0.04% compared to the dry R1 run. While conducting the research for this paper, we found that a 0.14% change in initial AH masses of the punctures resulted in a change in merger time of $6.7M$. Although we do not include simulations with such a large deviation of masses, we used this knowledge and assumed the change in merger time was linear in the change in initial mass to estimate an error.

4. *Proper Separation:* As mentioned in § III, the presence of the additional gravitational radiation also increased the proper separation, L , from the dry R1 $9.94M$ by up to 2.9%. We studied the effect of this change by evolving two BBH spacetimes with the same initial masses and angular momentum but increasing the coordinate to yield proper separations of $10.24M$ and $10.10M$. The merger time changed by at most $2.1M$. We assumed a linear relationship between the ΔT and ΔL in estimating the errors from this source at each data point.

The error bars presented in our figures are calculated by adding all the errors in quadrature:

$$\Sigma_{\Delta T}^2 = \Sigma_T^2 + \Sigma_{T_0}^2 \quad (8a)$$

$$\Sigma_T^2 = \left(\frac{\Delta T}{\Delta L} \Delta L\right)^2 + \left(\frac{\Delta T}{\Delta m} \Delta m\right)^2 + \Sigma_{\text{res}}^2 + \Sigma_{\text{tet}}^2,$$

where $\Sigma_{\Delta T}$ is the error in ΔT , Σ_T is the error in

T , and Σ_{T_0} is the error in T for the dry R1 run. $\Sigma_{\text{res}} = 0.75$ and $\Sigma_{\text{tet}} = 0.4$ are the largest measurements for the resolution and extraction radius errors. The accumulated errors do not account for the observed ΔT when $E_{\text{ADM}}/E_{\text{R1}} > 0.01$ and we note that the errors grow as the amplitude increases and the width decreases, most notably the errors associated with changes in the irreducible masses.

The parameter space of adding spurious radiation is large. In Table II, we present the results from a few evolutions outside of our main parameter survey. The junk radiation present in the initial data of a typical BBH simulation may not be well represented by an $\ell = m = 2$ mode. Similarly the effect of the junk radiation might be sensitive to the wavelength of the pulse. In order to test how important a modulation in the frequency might be to our conclusions, we briefly investigated an Eppley packet modulated with a cosine wave, given by

$$F(u) = A \cos(ku) u e^{-u^2/\sigma^2}. \quad (9)$$

This modulation adds an extra parameter controlling the wavelength of the perturbation. We adjusted the amplitude of the wave to keep the energy approximately comparable to our standard runs. The resulting simulation merger time differed from the unmodulated packet by less than $1M$ in T , well within error bars. While this is still an avenue open to investigation, we concluded that the modulation was not affecting the results enough to warrant an additional parameter in our survey. We also conducted a test of the geometry of the wave by initiating a pulse with an $\ell = 2$, $m = 0$ mode. Again we changed the amplitude so that the energy in the wave was approximately constant and found that there was a change in merger time of $1M$ compared to the $\ell = 2$, $m = 2$ simulation, again within error bars. This points towards the wavelength and angular dependence of the pulse being secondary to the additional energy in determining the effect of the pulse on the merger time.

Finally, to make a stronger connection to the junk radiation being associated with each puncture, we added *two* identical waves centered at each of the black holes rather than at the center. Compared to the same wave initiated at the center, the dual waves added almost twice the energy and almost doubled the change in merger time, which is consistent with the center-of-mass TNW.

A/M^3	σ/M	M_k	m	$\frac{E_{rad}}{E_{ADM,i}}$	$\frac{J_{rad}}{J_{ADM,i}}$	M_f	$\Delta T/M$
1	3	0	2	0.0696	0.252	0.970	-65.5
0.25	3	0	2	0.0382	0.272	0.970	-5.6
0.15	3	0	0	0.0382	0.271	0.961	-6.9
3×10^{-3}	4	2	2	0.0363	0.272	0.962	-4.5
7×10^{-4}	4	3	2	0.0358	0.272	0.962	-4.0
Dual 0.5	4	0	2	0.0411	0.271	0.960	-8.9

TABLE II: Overview of the odd runs. The left four columns are the wave parameters, followed by the fraction of ADM energy radiated and the fraction of the ADM angular momentum radiated. The final masses are given in the 7th column followed by the merger time change as derived by the peak of the waveform extracted at $75M$.

B. Dynamical and Radiated Quantities

We now investigate the effects of the TNWs on the radiated quantities derived from the waveforms. We calculate these quantities from the Weyl scalar Ψ_4 assuming, as in the calculation of the waveform, the fiducial tetrad of Baker et al. [26]. A summary of the quantities obtained from Ψ_4 are listed in Table I. The fraction of the initial ADM energy radiated was calculated across a detector at $40M$. As expected, the radiated energy increases with the strength of the wave. When $A < 0.5M^3$ and $\sigma \geq 5M$, there is no measurable difference between the BBH+TNW and the BBH cases within numerical error. For those cases, we can only conclude that the energy in the wave propagates out without a measurable interaction with the black holes. Similarly a trend emerges as we increase A for each σ , which corresponds to increasing E_{ADM} . The radiated angular momentum consistently decreases.

To look at the interaction of the TNW with the black holes as it propagates out, we study the radiated energy and angular momentum as functions of time. In Fig. 7 we plot the energy radiated across a detector at radius $r = 40M$. We see the energy grows from a time of $40M$ to around $80M$ as the initial burst of spurious radiation passes the detector. After this burst of energy the remaining energy radiated is approximately $0.035E_{ADM,R1}$ and is almost uniform across the various cases. From this we can see that most of the energy introduced in the spacetime is quickly flushed out of the system, leaving a system which radiates a further amount of energy that is independent of the junk radiation.

All the evolutions started from spacetimes with

equal J_{ADM} since the TNW does not add angular momentum to the BBH spacetime. In column five of Table I and in Fig. 8, we see that the amount of angular momentum radiated across a detector located at $40M$ is independent of the wave with some numerical error. The difference in J_{rad} between the runs lies in *when* the system radiates the angular momentum. This is better seen in Fig. 9 where we present the angular momentum flux across the sphere at $r = 40M$ and in Fig. 10, a close-up of the initial part of the data. The spurious radiation is transporting extra angular momentum as it is flushed out.

Figs. 7 and 8 show some of the TNW propagating out at the same time as the spurious radiation is flushing out. One of the consequences of the wave traveling away from the center of the orbit is that it can interact with the black holes and potentially increase the mass of each black hole during the early part of the inspiral. Table III documents how the AH masses change as a function of A and σ for the stronger TNW cases. The black-hole mass is calculated using an AH tracker [27]. The Δm is a measure of the change in the mass of each black hole up to $50M$, such that $\Delta m = m(t = 50M) - m(t = 0)$. The change in the initial ADM energy compared to the R1 run is given by $\Delta M = E_{ADM} - E_{ADM,R1}$ at $t = 0$. We use this estimate of the differences in the mass of the spacetime between R1 and the rest of the runs to compute a naive estimate of the total fraction of energy absorbed by both black holes. Up to 7.89% of the extra ADM energy is observed to

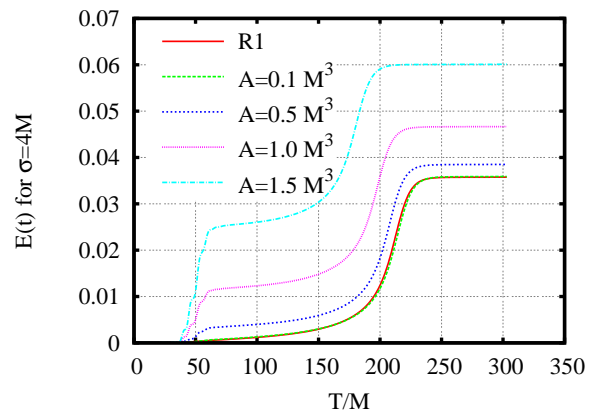


FIG. 7: Energy radiated across a sphere of radius $r = 40M$ as calculated from the Weyl scalar Ψ_4 .

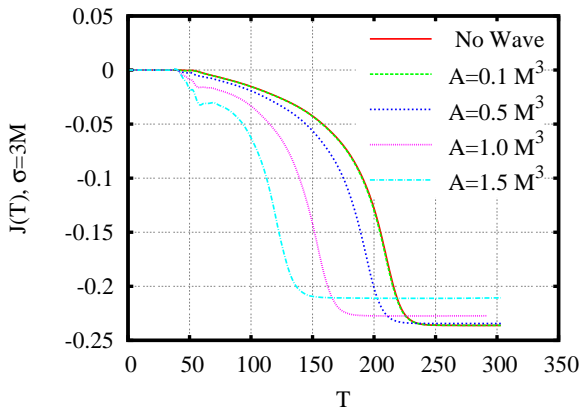


FIG. 8: Angular momentum radiated across a sphere of radius $r = 40M$ for σ of $3M$ as calculated from the Weyl scalar Ψ_4 .

be absorbed by the black holes during the first $50M$ of the simulation, 3.9% by each black hole. The actual amount absorbed depends strongly on the width of the wave: the narrow, strong pulses are more readily absorbed than the weak, diffuse pulses that extend beyond the black holes in the initial data. In the weaker cases the change is barely visible above the noise in the AH mass calculation, in the stronger cases it is unmistakable.

To assess how important the absorption of energy by the black holes during the evolution is to the changes in merger time and radiated angular momentum, we refer to our discussion about the sensitivity of the merger time to a change in the initial AH masses in § IV A. Given a change in mass of the individual black holes of 0.14%, the merger time changed by $6.7M$. In setting up the initial data, we do not allow the AH masses to change more than 0.04%. The amount of absorption measured during the evolution is as much as 3.9%; and, therefore, the increase in mass may be accounting for some, although not all, of the effects of the TNW. The outliers, the cases of most extreme merger times, merge so quickly that differentiating the burst of spurious radiation and region of pure inspiral is difficult. We also tried normalizing the time axis by the total AH masses after the wave has passed rather than that from the initial spacetime. This changed ΔT by no more than $1M$ so the choice of normalization does not account for the observed difference in merger times.

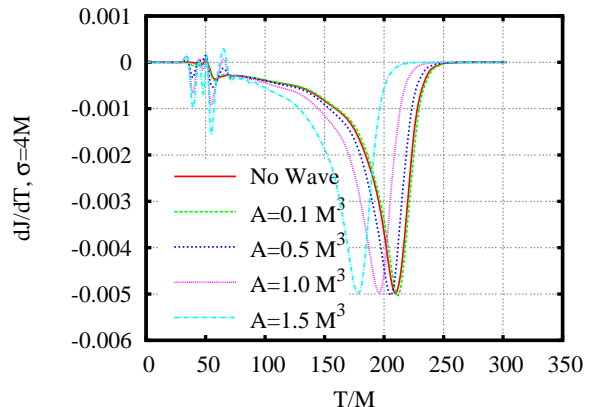


FIG. 9: Flux of angular momentum across a sphere of radius $r = 40M$ for σ of $4M$ as calculated from the Weyl scalar Ψ_4 .

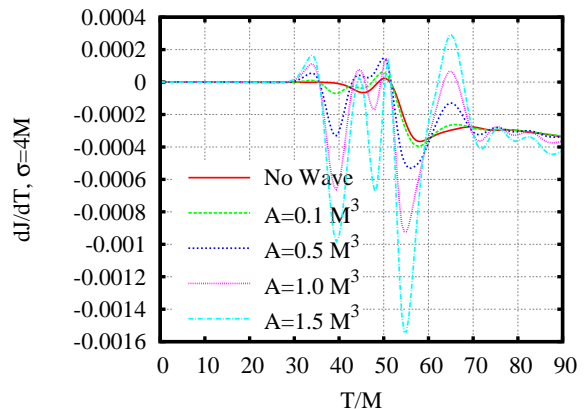


FIG. 10: Closeup of angular momentum flux across a sphere of radius $r = 40M$ concentrating on what the spurious radiation carries.

C. Final Spacetime

One of the important products of a BBH coalescence to relativists and astrophysicists are the final black hole's mass and spin. The final black hole masses and spins are presented in the last two columns of Table I. To compute the final mass, M_f , we use energy conservation arguments by calculating the difference between the ADM energy and the radiated energy as calculated from the Weyl scalar Ψ_4 . The final spin, $j_f = a_f/M_f$, is calculated by finding the complex ringdown frequency in the $\ell = 2$, $m = 2$ mode and using the numerical Kerr frequencies given in Table II of Appendix D in Berti et al [28] to find the correspond-

Masses					
A/M^3	σ/M	$\Delta m/M$	$\Delta M/M$	$2\Delta m/(\Delta M)$	$M_f/(2m(t=50))$
0	-	0	0	0	0.950
0.5	3	3.90×10^{-4}	0.0106	7.34×10^{-2}	0.950
1.0	3	1.56×10^{-3}	0.0412	7.57×10^{-2}	0.951
1.5	3	3.49×10^{-3}	0.0886	7.89×10^{-2}	0.953
1.0	4	2.84×10^{-4}	0.0113	5.03×10^{-2}	0.950
1.5	4	6.41×10^{-4}	0.0251	5.11×10^{-2}	0.949
1.0	5	5.89×10^{-5}	0.0045	2.62×10^{-2}	0.950
1.5	5	1.26×10^{-4}	0.0092	2.74×10^{-2}	0.950
1.0	6	1.76×10^{-5}	0.0020	1.76×10^{-2}	0.950

TABLE III: Change in AH mass compared to the difference in initial ADM energy for the stronger waves. Δm is the change in a single black hole AH mass over the first $50M$, ΔM is the additional ADM energy compared to the dry R1 run. Column 5 is the fraction of the extra ADM energy absorbed by both black holes combined, and the last column is the ratio of the final black hole mass to the total AH mass after the wave has been absorbed.

ing spin parameter. This method agrees within stated errors to inverting the fit of Eq. (E2) of the same paper. Given the strong dependence of the spin on the damping time, we limit ourselves to the real part of the complex frequency and compare this to a separate spin calculation using the isolated horizon framework [29] where possible.

From the values of M_f and j_f listed in Table I, we can see that the final spins are constant within numerical accuracy and the final masses do not vary strongly with A and σ . The trend is an increase in the final mass with increasing E_{ADM} becoming noticeably greater than our numerical errors for the four largest cases, $M_f \geq 0.963$. From this we can see that the narrower pulses not only have more energy, but they also interact more efficiently with the black holes. Being more readily absorbed by the punctures, they increase the individual masses and thus the final mass. The last column of Table III shows the ratio of the final mass to the total AH mass once the wave has interacted with the inspiraling black holes. We see the ratio is roughly constant, implying that approximately 5% of the initial AH mass is radiated away *if* we include the wave energy absorbed by the black holes. The exception is the most extreme wave where the black holes merged before all the spurious radiation has been absorbed into the AH. This would underestimate the AH growth and thus overestimate the value of the ratio. The change in final mass agrees within numerical error to the change in total AH mass after the wave has

interacted with the inspiraling black holes except for the case of the strongest wave. In that case the AHs have not absorbed all the energy before the black holes begin to merge so we are underestimating the growth of these black holes.

D. Alignment of Amplitude and Phase

As stated in the introduction, a common method to compare waveforms is via a time-shift of the amplitude of each waveforms such that their peaks overlap, the result of which is shown in Fig. 11. We can see that the waveforms overlap very well after the merger. The only noticeable difference is for the strongest TNW we evolved on the BBH system, the $A = 1.5M^3$, $\sigma = 3M$ case, where we find the largest difference in the final black hole compared to the dry R1 run. We can also see residual contamination of the merger portion of the waveform by the spurious radiation due to the binary merging so quickly. Similarly, we shift the waveform phase such that they overlap at $T = T_{\text{peak}}$ in Fig. 12. The agreement in the phase's slope during ringdown is further confirmation that the mass and spin of the final black hole are not significantly altered.

The waveform overlap in the merger regime continues to start before the merger, as seen in [10], as long as the spurious radiation does not contaminate this region of the waveform. This alludes to the relatively simple form of the merger waveform seen in all the various situations currently tested. As long as the spurious radiation is not strong enough to noticeably alter the final black hole, the merger portion of the waveform remains essentially unaltered and the contamination to the system predominately results in the change in merger time and thus a time-shift of the waveform.

V. CONCLUSIONS

In this study, we simulated an equal-mass, non-spinning BBH system through its last orbits, merger and ringdown. The system is perturbed by the systematic addition of spurious radiation in the form of a Teukolsky-Nakamura gravitational wave at the binary's center of mass. The initial energy of the wave is tunable, specified by the amplitude and width of the radiation; in addition, the initial angular momentum was fixed for the entire

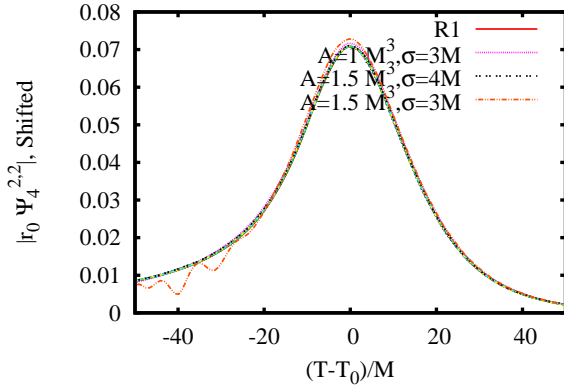


FIG. 11: Comparison of $|\Psi_4^{2,2}|$ for all runs shifted such that the peak amplitudes before ringdown coincide. This lets us compare the relative damping times of the ringdown and thus the properties of the final black hole. We also note the agreement for about $50M$ before ringdown as well. Though the legend only labels the distinguishable cases, all the runs are contained in the figure.

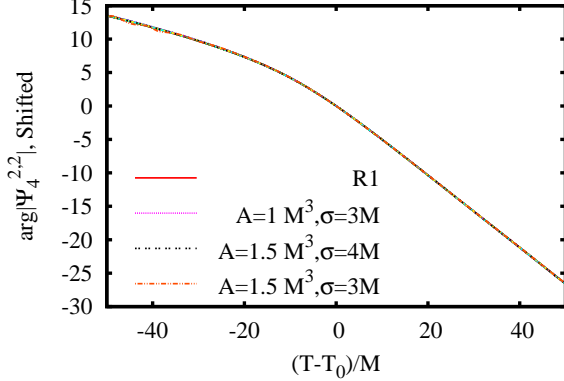


FIG. 12: Comparison of $\arg(\Psi_4^{2,2})$ for all runs shifted such that the peak amplitudes before ringdown coincide and shifted vertically. This lets us compare the relative frequencies of ringdown. Though the legend only labels the distinguishable cases, all the runs are contained in the figure.

sequence of runs. The binaries that contain the extra radiation invariably merge faster than those with no additional radiation.

In addition to the main result of decreasing merger time, some changes to the radiated quantities and the final black hole were measurably

above numerical error. This occurred once the additional energy provided by the TNW was equal to or greater than 1% of the dry BBH spacetime. As the TNW propagated out of the center, approximately 4% of additional ADM energy was absorbed by each black hole. In that strong-wave case, it was not possible to make an accurate measurement of the mass of the enlarged black holes before the plunge of the binary. The final spins of the black holes, however, remained unaffected by the gravitational radiation for all but the strongest case ($A = 1.5M^3$, $\sigma = 3M$). The constant black-hole spin is consistent with the wave slightly increasing the eccentricity of the orbit for small eccentricities [30, 31]. We also observed a decrease in the radiated angular momentum with increasing TNW strength.

We conjecture, based on the change in the initial binding energy of the BBH+TNW systems and Newtonian back-of-the-envelope calculation, that the spurious radiation increases the eccentricity of the original orbit. Unfortunately, the separation of the black holes was not large enough to enable a reliable calculation of the eccentricity. The merger time is very sensitive to the increase in individual black-hole masses via wave absorption; however, this was not enough to account for the observed change in the time of merger even when ignoring the strongest wave case. The combined effects of increasing the individual black-hole masses and the eccentricity of the orbit caused the binaries to merge faster with increasing energy.

One of the conjectures in the literature is that the spurious radiation, intrinsic to the construction of initial data for BBH evolutions, is flushed out of the simulation within a crossing-time and does not effect the radiation or the binary. We can relate the results of this study to other BBH evolutions by looking at the early changes in AH mass as well as how much energy leaves the system in the burst of spurious radiation. For the dry R1 run, the energy radiated in the initial pulse is $9 \times 10^{-4} E_{\text{ADM},R1}$. We find that there is negligible effect on the merger time at that level. Our results indicate that the spurious radiation present in initial data sets is unlikely to cause dramatic departures from the true BBH solution and therefore we can state that the simulated merger is robust to the presence of spurious radiation.

Acknowledgments

This work was supported in part by NSF grants PHY-0653443, PHY-0555436 and PHY-0114375 (CGWP). Computations were performed at NCSA and TACC under allocation TG-PHY060013N, and at the Information Technology Services at

Penn State. The authors thank M. Ansorg, E. Bentivegna, A. Knapp, P. Laguna, R. Matzner, E. Schnetter, U. Sperhake and J. Thornburg for contributions to the computational infrastructure and helpful discussions, and E. Berti for the data tables used in the quasi normal fitting.

-
- [1] H. P. Pfeiffer, D. A. Brown, L. E. Kidder, L. Lindblom, G. Lovelace, and M. A. Scheel, *Classical Quantum Gravity* **24**, S59 (2007).
 - [2] F. Pretorius, *Phys. Rev. Lett.* **95**, 121101 (2005).
 - [3] J. G. Baker, J. Centrella, D. Choi, M. Koppitz, and J. van Meter, *Phys. Rev. Lett.* **96**, 111102 (2006).
 - [4] M. Campanelli, C. O. Lousto, P. Marronetti, and Y. Zlochower, *Phys. Rev. Lett.* **96**, 111101 (2006).
 - [5] F. Herrmann, I. Hinder, D. Shoemaker, and P. Laguna, *Class. Quant. Grav.* **24**, S33 (2007).
 - [6] J. A. Gonzalez, U. Sperhake, B. Brügmann, M. Hannam, and S. Husa, *Phys. Rev. Lett.* **98**, 091101 (2007).
 - [7] M. Koppitz, D. Pollney, C. Reisswig, L. Rezzolla, J. Thornburg, P. Diener, and E. Schnetter, *Phys. Rev. Lett.* **99**, 041102 (2007).
 - [8] W. Tichy and P. Marronetti, *Phys. Rev. D* **76**, 061502(R) (2007).
 - [9] J. G. Baker, J. Centrella, D.-I. Choi, M. Koppitz, and J. van Meter, *Phys. Rev. D* **73**, 104002 (2006).
 - [10] J. G. Baker, M. Campanelli, F. Pretorius, and Y. Zlochower, *Class. Quant. Grav.* **24**, S25 (2007).
 - [11] U. Sperhake, *Phys. Rev. D* **76**, 104015 (2007).
 - [12] M. Campanelli, C. O. Lousto, and Y. Zlochower, *Phys. Rev. D.* **73**, 061501(R) (2006).
 - [13] D.-I. Choi, B. J. Kelly, W. D. Boggs, J. G. Baker, J. Centrella, and J. van Meter, *Phys. Rev. D* **76**, 104026 (2007).
 - [14] M. Hannam, S. Husa, B. Brügmann, J. A. González, and U. Sperhake, *Class. Quant. Grav.* **24**, S15 (2007).
 - [15] B. Vaishnav, I. Hinder, F. Herrmann, and D. Shoemaker, *Phys. Rev. D* **76**, 084020 (2007).
 - [16] S. Brandt and B. Brügmann, *PRL* **78**, 3606 (1997).
 - [17] M. Ansorg, B. Brügmann, and W. Tichy, *Phys. Rev. D* **70**, 064011 (2004).
 - [18] K. S. Thorne, *Rev. Mod. Phys.* **52**, 299 (1980).
 - [19] S. A. Teukolsky, *Phys. Rev. D* **26**, 745 (1982).
 - [20] T. Nakamura, K. Oohara, and Y. Kojima, *Prog. Theor. Phys. Suppl.* **90**, 1 (1987).
 - [21] K. Eppley, in *Sources of Gravitational Radiation*, edited by L. L. Smarr (Cambridge University Press, Cambridge, UK, 1979), pp. 275–291, ISBN 0-521-22778-X.
 - [22] J. W. York, in *Sources of Gravitational Radiation*, edited by L. L. Smarr (Cambridge University Press, Cambridge, UK, 1979), pp. 83–126, ISBN 0-521-22778-X.
 - [23] J. M. Bowen and J. W. York, *Phys. Rev. D* **21**, 2047 (1980).
 - [24] E. Pazos, E. N. Dorband, A. Nagar, C. Palenzuela, E. Schnetter, and M. Tiglio, *Class. Quant. Grav.* **24**, S341 (2007).
 - [25] L. Lehner and O. M. Moreschi, preprint (arXiv.org:0706.1319) (2007).
 - [26] J. Baker, M. Campanelli, and C. Lousto, *Phys. Rev. D* **65**, 044001 (2002).
 - [27] J. Thornburg, *Class. Quant. Grav.* **21**, 743 (2004).
 - [28] E. Berti, V. Cardoso, and C. M. Will, *Phys. Rev. D* **73**, 064030 (2006).
 - [29] O. Dreyer, B. Krishnan, E. Schnetter, and D. Shoemaker, *Phys. Rev. D* **67**, 024018 (2003).
 - [30] I. Hinder, B. Vaishnav, F. Herrmann, D. Shoemaker, and P. Laguna, preprint (arXiv:0710.5167) (2007).
 - [31] U. Sperhake, E. Berti, V. Cardoso, J. A. Gonzalez, B. Brügmann, and M. Ansorg, preprint (arXiv:0710.3823) (2007).